Multiphase CFD Simulations of Solid Propellant Combustion in Gun Systems

Michael J. Nusca and Paul J. Conroy
Weapons and Materials Research Directorate, Army Research Laboratory
Aberdeen Proving Ground, MD 21005

Abstract

The Army Research Laboratory has developed a scaleable, 3D, multiphase, computational fluid dynamics (CFD) code with application to gun propulsion (interior ballistics) modeling. The NGEN3 code, which incorporates general continuum equations along with auxiliary relations into a modular code structure, is readily transportable between computer architectures and is applicable to a wide variety of gun propulsion systems. Two such systems are the Army's Modular Artillery Charge System (MACS) and the Future Combat System (FCS). The MACS is being developed for indirect fire cannon on both current and developing (e.g., Crusader) systems. The efficiency of the MACS charge is dependent on proper flamespreading through the propellant modules; a process that has been repeatedly demonstrated in gun firings, successfully photographed using the ARL ballistics simulator, and numerically modeled using the NGEN3 code. The FCS requires weapons systems exhibiting increased range and accuracy. One of the technologies under investigation to achieve these goals is the electrothermal-chemical (ETC) propulsion concept, in which electrically generated plasma is injected into the gun chamber igniting the high-loading-density (HLD) solid propellant charge. NGEN3 code development and application to the MACS and FCS is currently a DoD HPC Grand Challenge (No. 112) and is being greatly advanced by access to the DoD high performance computers (HPCs).

Introduction

A solid propellant gun system consists of a reaction chamber connected to a gun tube through which a projectile is guided once propelled by pressurization of the chamber. Chamber pressurization is accomplished by placing a solid propellant (SP) charge in the chamber and igniting it by various means. Current SP charges are generally complex structures consisting of hundreds or even thousands of distinct regularly formed (e.g., spherical, cylindrical) grains, which may be loaded in either regular or random arrangements. In addition to small-scale voidage between grains (i.e., porosity) many charges also contain large-scale voidage (i.e., ullage), which surrounds the entire charge (such as when the charge does not fill the entire chamber volume) or separates distinct subcharges (i.e., increments or modules) that together comprise the whole charge. The addition of energy to the chamber, usually near the gun breech, or rearmost end of the chamber, and in some cases through a tube extending along the centerline of the chamber, ignites the SP. In general, all of the grains are not ignited simultaneously, but an ignition flame spreads from the breech to the projectile base. The burning of the SP transforms chemical energy into heat as hot gases evolve from the surface of each grain of propellant. Initially the projectile resists movement allowing the pressure in the chamber to climb rapidly. Since the burn rate of the propellant is proportional to the pressure, hot gases are produced at an accelerated rate until peak pressure is reached in the chamber. Movement of the projectile down the gun tube, usually slight before peak pressure and much more significant afterwards, causes the chamber volume to increase, and

generates rarefaction waves, which lower the pressure and thus the burn rate of the propellant. Upon ignition and burning, the gas dynamic flowfield in the gun chamber takes on a highly complex structure that includes the dynamics of propellant motion and combustion and various gas dynamic flow phenomena such as turbulent mixing, highly transient pressure waves, steep gradients in porosity and temperature, non-ideal thermodynamics, and gas generation.

As a direct result of the complexity of the interior ballistic event, briefly described above, numerical simulation of the multiphase gas dynamics and propellant combustion in a gun chamber is critically important to gun charge design. In some cases a new charge design is not performing as planned and numerical simulations are used to elucidate the important physics involved during flamespreading in the SP and augment experimental data gathering during gun firings. These efforts commonly lead to subtle charge design changes that increase the efficiency of the new design. In other cases a new charge design can generate pressure waves of dangerously high levels that inappropriately stress the gun system. A central goal in computer modeling of the interior ballistics event is to predict the maximum pressure in the chamber and the projectile's gun tube exit velocity (or muzzle velocity). For some SP charges, successful modeling can be accomplished using one-dimensional, single-phase, "lumped parameter" models, which are based on the assumption that grains and the products of combustion constitute a well-stirred mixture. However, it has long been recognized that many charges, especially those involving multiple increments and complex distributions of ullage, the effects of which are nonuniformities in certain interior ballistic events (e.g., ignition, flamespreading), can only be simulated on the basis of a multidimensional multiphase flow model. In an ETC gun, the plasma injection event and the resulting plasma convection, diffusion and participation in ignition and flamespreading, through the SP, is also most accurately simulated using a multidimensional multiphase flow model.

Building on a successful history of gun propulsion modeling and simulation, the Army Research Laboratory has developed a next generation interior ballistics model, NGEN3, which incorporates three-dimensional continuum equations along with auxiliary relations into a single code structure that is both modular and transportable between scaleable computer architectures. Since interior ballistics involves flowfield components of both a continuous (i.e., air and gaseous combustion products) and a discrete (i.e., solid propellant) nature, an Eulerian/Lagrangian approach is utilized. On a sufficiently small scale of resolution in both space and time, the components of the flow are represented by the balance equations for a multicomponent reacting mixture describing the conservation of mass (global and species), momentum, and energy. A macroscopic representation of the flow is adopted using these equations derived by a formal averaging technique applied to the microscopic flow. The numerical representation of these equations and constitutive laws, as well as the numerical solution thereof, is based on a finite-volume discretization and high-order accurate, conservative solution schemes.

The Grand Challenge – Motivation for the Project

The Army requires gun propulsion charges for both legacy systems (i.e., in-direct fire cannon employing the Modular Artillery Charge System, MACS) and the Future Combat System, FCS (i.e., direct-fire weapons employing high-loading density charges). Development of the propelling charges for

these systems requires advanced physics-based modeling. Until the advent of the NGEN3 code, the gun propulsion-modeling environment was one in which separate codes were used to analyze different propulsion schemes, with no single code able to address several systems. This situation rendered comparison of ballistic performance for various systems cumbersome and inconclusive. In contrast, the multiphase continuum equations that represent the physics of gun propulsion comprise a set of general equations applicable to gun propulsion systems in general. Thermodynamic state equations and constitutive laws, as well as boundary conditions represent differences in system details. The ARL's NGEN3 multiphase CFD code for solid propellant combustion represents the sole DoD code that is able to simulate the highly complex physics associated with indirect- and direct-fire guns. The NGEN3 code includes validated subroutines for both modularly packaged granular charges and high-loading density (HLD) charges in which various SP media are employed. In addition, the NGEN3 code includes plasma injection and mixing models. The ARL is therefore poised to use high-performance computers (HPCs) to impact the development of new gun charges and gun systems that will be the subject of intense research and development for many years.

The Army's Modular Artillery Charge System (MACS) is the propulsion system for all fielded 155mm guns including the Crusader cannon. The MACS charges are designed to both significantly increase muzzle energy and to be suitable for application in automated loading systems. As a result of the modular charge design there is a physical barrier (i.e., the case) at the interface between two adjacent charge increments. Since direct ignition transfer is therefore impeded, charge ignition may not proceed in the order in which the charges are loaded into the gun chamber without a highly effective ignition system. These system-specific details (such as the propellant module cases and igniters) must be modeled as part of the overall numerical simulation and cannot be accurately treated with less than a multi-dimensional CFD code (i.e., 1D "lumped-parameter" models cannot properly model the MACS). The efficiency of the MACS charge is highly dependent on proper flamespreading through the modules, which can only be modeled using the NGEN3 code since ignition, and flamespreading in the MACS charge is largely three-dimensional. Data from experimental pressure taps located on the gun chamber wall and even photographs and movies of the MACS in the ARL's clear-tube ballistic simulator do not provide enough detail, in some cases, to diagnose the performance of the MACS charge. PM-Crusader, recognizing the vast importance of numerical simulations, has increased demand on the NGEN3 code. It is one of the ARL's top mission priorities to support PM-Crusader and the ARDEC.

The Army's Future Combat System (FCS) requires weapons systems exhibiting greater range and accuracy. Several technologies are under investigation in order to achieve these goals. HLD charges consist of SP cast in several media types (e.g., grains, sticks, and disks) combined into a single charge. These combinations along with small-scale gaps between SP media and large-scale ullage around the projectile afterbody create special concerns for efficient ignition and flamespreading in the HLD charge. A promising ignition technology for HLD charges is the Electrothermal-Chemical (ETC) concept. In the ETC gun, energy, which is stored either in batteries or a rotating device, is converted on demand into an electrically generated plasma (resulting from the ablation of polyethylene material in a capillary) that is injected into the chamber in a howitzer or gun. This plasma energy is used to ignite the chemical

propulsion charge (e.g., solid propellant) as well as to enhance gun performance by taking advantage of a number of unique plasma characteristics. For example, a low density plasma jet can efficiently ignite charges of high loading density, can control propellant mass generation rates, can reduce propellant charge temperature sensitivity, i.e., the variation of gun performance with changing ambient temperature and can shorten ignition delay, i.e., the time interval between firing of the igniter and ignition of the propellant. Plasma igniters also eliminate the conventional chemical igniter and thus can enhance the safety aspects of the overall gun propulsion system. All of these observations have a significant effect on the ballistics of ETC gun systems and can lead to a useful improvement in gun performance and accuracy.

NGEN3 CFD Code Description

The NGEN3 code has been documented elsewhere by Nusca and Gough [1,2,3]. The governing equations, state equations and constitutive relations are based on the works of Gough and Zwarts [4] and Gough [5]. The two-dimensional version of the code (physical and numerical models) is described herein. Extensions to three-dimensions are described elsewhere [3].

Physical Model

Since interior ballistics involves flowfield components of both a continuous (i.e., air and gaseous propellant combustion products) and a discrete (i.e., solid propellant) nature, a Eulerian/Lagrangian approach is utilized, based on a solution of the conservation equations for a multiphase reacting flow. Two phases are considered, a continuous phase (multicomponent mixture of gases in local mechanical equilibrium), and a discrete phase (aggregate of particles made up of solid propellant grains). On a sufficiently small scale of resolution in both space and time, the components of the flow are represented by the balance equations for a multicomponent mixture describing the conservation of mass (global and for each species), momentum, and energy. The configuration (i.e., particle size and number) of the discrete phase makes the governing equations computationally intractable. Therefore, a **macroscopic** representation of the flow is adopted using the balance equations derived by a formal averaging technique applied to the **microscopic** flow. These equations require a number of constitutive laws for closure including molecular transport terms, state equations, chemical reaction rates, intergranular stresses, and interphase transfer of energy, momentum, and mass. In addition, the morphology of the discrete phases is required and is typically expressed as a surface area per unit volume of each particle. The numerical representation of these balance equations and constitutive laws, as well as the numerical solution thereof, is described in the section titled Numerical Model.

Multiphase Governing Equations

A general overview of the multiphase governing equations as they apply to interior ballistics is given by Gough [4,5]. A brief description is included herein. The flowfield may be viewed as consisting of a multicomponent fluid, referred to as the continuous phase, and the discrete phase. The continuous phase is understood to be a multi-component mixture of gases and droplets or particles that are small

enough to ensure local mechanical equilibrium. The gases are always in local thermal equilibrium while the droplets and particles are not necessarily so. The continuous phase is characterized by single local values of density, ρ, velocity vector, $\mathbf{u}$, temperature, T, pressure, p, shear stress tensor, τ, and internal energy, e. It is assumed to comprise N_C species each characterized by local values of mass fraction, Y_i. Moreover, the velocity, $\mathbf{u}$, is understood to be the barycentric or mass weighted average of the velocities of each of the components [6]. Each component is characterized by a diffusion velocity, $\mathbf{v_i}$, relative to the barycentric value, $\mathbf{u}$. The discrete phase is understood to refer to an aggregate of particles or droplets consisting of a total of N_d components. Each component is characterized by density, $\rho_{d,i}$, stress tensor, $\sigma_{d,i}$, velocity vector, $\mathbf{u}_{d,i}$, temperature, $T_{d,i}$, number density, $n_{d,i}$, and morphological data to characterize the volume, $V_{d,i}$, and surface area, $S_{d,i}$, of each particle or droplet. The temperature, $T_{d,i}$, may be either a surface or a bulk temperature.

The macroscopic formulation of the balance equations is such that it reduces to standard continuum equations in the context of single-phase flow. Given a microflow property ψ then $\langle\psi\rangle$, $\langle\psi\rangle_\rho$, and $\langle\psi\rangle_s$, are used to respectively denote a bulk average, a mass-weighted (Favre) average and an interphase surface average. The porosity, or the fraction of a unit macroscopic volume occupied by the continuous phase is denoted by α. Similarly, $\alpha_{d,i}$ is used to denote the volume fraction of the i-th discrete phase. Evidently, $\alpha = 1 - \Sigma\,\alpha_{d,i}$, with the sum over all discrete components, N_d. The balance equation for mass is given by,

$$\frac{\partial}{\partial t}\left[\alpha\langle r\rangle\right] + \nabla\bullet\left[\alpha\, r\,\langle\mathbf{u}\rangle_r\right] = \sum_{i=1}^{N_d}\dot{m}_{di} \tag{1}$$

where $m_{d,i}$ is the rate of decomposition per unit volume of the i-th discrete phase. Each of the j components of the continuous phase satisfies a balance of mass equation in the following form,

$$\frac{\partial}{\partial t}\left[\alpha\langle r\rangle\langle Y_j\rangle_r\right] + \nabla\bullet\left[\alpha\langle r\rangle\langle Y_j\rangle_r\left(\langle\mathbf{u}\rangle_r + \langle\mathbf{v}_j\rangle_r\right)\right] = \alpha\langle\dot{w}_j\rangle + \sum_{i=1}^{N_d}\left(\dot{m}_{di}\right)\langle Y_{di}\rangle_s \tag{2}$$

where $\langle w_j\rangle$ is the average rate of production per unit volume of species j by chemical reactions and $\langle Y_{d,ij}\rangle_s$ is the average mass fraction of species j produced by the decomposition of the i-th discrete phase including the effect of the surface reaction. The macroscopic balance of momentum for the continuous phase takes the form,

$$\frac{\partial}{\partial t}\left[\alpha\langle r\rangle\langle\mathbf{u}\rangle_r\right] + \nabla\bullet\left[\alpha\langle r\rangle\langle\mathbf{u}\rangle_r\langle\mathbf{u}\rangle_r\right] = -\alpha\,\nabla\langle p\rangle + \alpha\,\nabla\bullet\langle t\rangle + \sum_{i=1}^{N_d}\left(\dot{m}_{di}\right)\langle u_{di}\rangle - \sum_{i=1}^{N_d}n_{di}\,S_{di}\,\mathbf{f}_{di} \tag{3}$$

where $\mathbf{f}_{di}$ represents the interphase drag due to the i-th discrete phase. The energy equation for the continuous phase takes the form,

$$\frac{\partial}{\partial t}\left[\alpha\langle r\rangle\left(\langle e\rangle_r + \frac{\langle u\rangle_r^2}{2}\right)\right] + \nabla\bullet\left[\alpha\langle r\rangle\langle\mathbf{u}\rangle_r\left(\langle e\rangle_r + \frac{\langle u\rangle_r^2}{2}\right)\right] = \nabla\bullet\alpha\langle u\rangle_r\bullet\langle s\rangle - \nabla\bullet\alpha\langle q\rangle - \langle p\rangle\frac{\partial\alpha}{\partial t}$$

$$- \sum_{i=1}^{N_d}n_{di}\,S_{di}\langle q_{di}\rangle_s - \sum_{i=1}^{N_d}n_{di}\,S_{di}\,\mathbf{f}_{di}\bullet\langle u_{di}\rangle_r + \sum_{i=1}^{N_d}\left(\dot{m}_{di}\right)\left(\langle e_{di}\rangle + \frac{\langle p\rangle}{\langle r_{di}\rangle} + \frac{\langle u_{di}\rangle^2}{2}\right) \tag{4}$$

Note that the phase interaction terms on the right hand side of Equation 4: heat transfer due to conduction and radiation per unit surface area $\langle q_{di}\rangle_s$, work done by the interphase drag, and heat

added due to decomposition of the discrete phases. The i-th discrete phase is governed by a macroscopic mass balance,

$$\frac{\partial}{\partial t}\left[a_i \langle r_{di}\rangle\right] + \nabla \bullet \left[a_i \langle r_{di}\rangle\langle \mathbf{u}_{di}\rangle_r\right] = - \dot{m}_{di} \tag{5}$$

analogous to Equation 1, and a macroscopic momentum balance equation,

$$\frac{\partial}{\partial t}\left[a_i \langle r_{di}\rangle\langle \mathbf{u}_{di}\rangle_r\right] + \nabla \bullet \left[a_{di} \langle r_{di}\rangle\langle \mathbf{u}_{di}\rangle\langle \mathbf{u}_{di}\rangle\right] = -a_{di}\nabla\langle p\rangle - \nabla \bullet \left[a_{di} \langle s_{di}\rangle\right] + n_{di} S_{di} \mathbf{f}_{di} - \left(\dot{m}_{di}\right)\langle \mathbf{u}_{di}\rangle_r \tag{6}$$

Note on the right hand side of Equation 6 the formal presence of a stress term, $\langle\sigma_{di}\rangle$, which reflects the difference between the average stress in the i-th discrete phase and the average ambient pressure in the continuous phase, interpreted as interactions between particles.

Constitutive Laws for the Continuous Phase

For simplicity of presentation consider the continuous phase to consist of a gas whose mass fraction is Y_g and a liquid phase whose mass fraction is $Y_L = 1 - Y_g$ and admit all values of Y_g between zero (all liquid) and one (all gas). The gas satisfies a covolume equation of state,

$$p = \frac{r_g R T}{\left(1 - b\, r_g\right)} \qquad \text{with} \qquad e = c_v T \tag{7}$$

where p is pressure, ρ_g is gas density, R is gas constant, T is temperature, b is covolume, e is internal energy and c_v is the specific heat at constant volume. For a mixture of gases the properties are computed in the usual composition dependent manner. Temperature dependence is not considered. The liquid is assumed to obey the law,

$$p = \frac{K_1}{K_2}\left[\left(\frac{r_L}{r_{Lo}}\right)^{K_2} - 1\right] \tag{8}$$

where K_1 and K_2 are empirical constants, ρ_L is the density and ρ_{Lo} is the density at ambient pressure. All liquid phases are assumed to be characterized by the same values of K_1 and K_2. The internal energy of the liquid follows from an integral of Equation 8.

The solution algorithm provides values of mixture density, ρ_m, and energy, e_m. Mixture pressure follows from a consideration of the volume fraction of the gases, ε, using,

$$r_g = Y_g\, r_m / e \quad ; \quad r_L = Y_L\, r_m / (1 - e) \tag{9}$$

where a value of ε is determined such that p values according to Equations 7 and 8 agree.

At present the model neglects diffusive processes in the continuous phase such as viscous effects and heat conduction. However, chemical reactions are admitted. In addition to Arrhenius reactions in the conventional form [6] a pressure dependent law and a shear strain dependent law are admitted. The pressure dependent law is applied to cases involving the combustion of droplets or small solid particles in the continuous phase mixture.

$$\left(\overset{\bullet}{\boldsymbol{w}}\right)= \frac{\boldsymbol{e}\,\boldsymbol{r}_m\,B\,p^{\,n}}{D_p} \qquad ; \qquad \overset{\bullet}{w} = k_s\,Y_L\,\boldsymbol{r}_m\,\left|\frac{\partial u}{\partial r}+\frac{\partial v}{\partial z}\right| \tag{10}$$

where D_p is the droplet diameter, assumed a fixed value, and k_s is a user specified coefficient.

Constitute Laws for the Discrete Phase

Certain constitutive laws associated with the presence of solid propellants are independent of the isotropy of the arrangement of the propellant. Briefly, these include the morphology of the propellant, or the surface area per unit volume; the burn rate, an exponential function of pressure; and the model of thermal response during the ignition phase, a local solution of the one-dimensional heat conduction equation driven by the interphase heat transfer as a boundary condition until a predetermined ignition temperature is achieved. The constitutive laws which depend on the isotropy of the propellant arrangement are the intergranular stress laws, or rheology; the interphase drag; and the interphase heat transfer. The laws listed herein apply to randomly packed granular propellants.

The intergranular stress is taken to depend on porosity, α, using, $\;a(\boldsymbol{a})=\left[\dfrac{-g_o}{\boldsymbol{r}_p}\dfrac{\mathrm{d}\boldsymbol{s}}{\mathrm{d}\boldsymbol{a}}\right]^{1/2}$

and the direction of loading as embedded into a formula for the rate of propagation of intergranular disturbances,

$$\frac{D\boldsymbol{s}}{D\,t_p} = -\frac{\boldsymbol{r}_p\,a^2\,\overset{\bullet}{\boldsymbol{a}}}{g_o} \quad (\text{isotropic}) \quad ; \quad \frac{D\boldsymbol{s}_{zz}}{D\,t_p} = -(1-\boldsymbol{e})\,\frac{\boldsymbol{r}_p\,a_z^2}{g_o}\left[\frac{\P u_p}{\P z}+\boldsymbol{n}_{zr}\frac{\P v_p}{\P r}+\boldsymbol{n}_{zq}\frac{v_p}{r}\right]\;(\text{anisotropic}) \tag{11}$$

where $a(\alpha)$ has been recast into an equation with a form that is more suitable for numerical integration. Both the isotropic and anisotropic forms are admitted. The Poisson ratios, ν_{zr} and $\nu_{z\theta}$ are taken as $1/3$ based on recent experimental data [7]. In order to formulate the functional behavior of $a(\alpha)$ introduce α_o, the settling porosity of the bed, and values of $a(\alpha)$ equal to a_1 and a_2 which respectively correspond to loading at α_o and to unloading/reloading. The nominal loading curve, corresponding to monotonic bed compaction from α_o to a smaller value α is given,

$$\boldsymbol{s} = \boldsymbol{s}_{\mathrm{nom}}(\boldsymbol{a}) = \boldsymbol{r}_{\mathrm{g}}\,\frac{a_1^2}{g_o}\,a_o^2\left(\frac{1}{a}-\frac{1}{a_o}\right) \tag{12}$$

with $a(\alpha) = \{\;a_1\alpha_o/\alpha\;(\text{for }\sigma=\sigma_{\mathrm{nom}})\;;\;a_2\;(\text{for }\sigma<\sigma_{\mathrm{nom}})\;;\;0\;(\text{for }\sigma=0)\;\}$. The interphase drag in a granular bed is given in the following form,

$$\mathbf{f}_s = \frac{1-\boldsymbol{a}_e}{D_{pe}}\left(\frac{\boldsymbol{a}}{\boldsymbol{a}_e}\right)^3\boldsymbol{r}\left|\mathbf{u}-\mathbf{u}_p\right|\left(\mathbf{u}-\mathbf{u}_p\right)\hat{f}_s \tag{13}$$

Equation 13 refers to the exterior voidage, α_e, and the effective diameter, D_{pe}, based on the grain exterior volume and surface area. In addition,

$$\left(\hat{f}_s\right) = C\left(\hat{f}_{s,RG}\right) = 0.85\left[2.5\,\mathrm{Re}_p^{-0.081}\,\boldsymbol{l}^{\,2.17}\right] \quad ; \quad \boldsymbol{l} = \frac{0.5+L/D}{\left(3L/\,2D\right)^{2/3}} \quad ; \quad \mathrm{Re}_p \equiv \frac{\boldsymbol{r}_f\left|\mathbf{u}-\mathbf{u}_p\right|D_{pe}}{\boldsymbol{m}_f}$$

Here L is the length of a cylindrical grain, D as its diameter, ρ_f and μ_f are the density and viscosity of the gas at the film temperature. The viscosity is taken to have a Sutherland-type dependence on temperature, $\mu = 0.134064(T/298)^{1.5}/(T+110)$.

The interphase heat transfer is assumed to be governed by an empirical correlation [8].

$$\mathrm{Nu}_p \equiv \frac{h\,D_p}{k_f} = 0.4\,\mathrm{Pr}^{1/3}\,\mathrm{Re}_p^{2/3} \quad ; \quad \mathrm{Pr} \equiv \frac{c_p\,\boldsymbol{m}}{k} = \frac{4\boldsymbol{g}}{9\boldsymbol{g} - 5} \quad ; \quad h = \frac{q}{T - T_p} \quad ; \quad q_p = (1 - \boldsymbol{a})\frac{qS_p}{V_p} \quad (14)$$

where $h = q/(T-T_p)$ as the film coefficient and q is the heat transfer per unit surface area. The subscript f denotes an evaluation of properties at the film temperature, $(T-T_p)/2$, where T and T_p are respectively the continuous phase bulk average temperature and the particle surface average temperature. The heat transfer per unit volume, q_p, is related to q by, $q_p = (1-\alpha)$ q S_p/V_p.

Assuming that ignition is an essentially uniform event with respect to the surface of each propellant grain and supposing that the temperature distribution within the solid phase can be captured by a cubic profile, leads to the following expression for the surface temperature,

$$T_p = T_{po} - \frac{2hH}{3\,k_p^2} + \left[\left(T_{po} - \frac{2hH}{3\,k_p^2}\right)^2 + \frac{4hTH}{3\,k_p^2} - T_{po}^2\right]^{1/2} \quad ; \quad \frac{DH}{Dt}_p = \boldsymbol{a}_p\,q \qquad (15),(16)$$

where T_{po} is the initial surface temperature. Ignition of the solid propellant grain is assumed to occur when the surface temperature exceeds a pre-determined value. The rate of surface regression is given by,

$$\dot{d} \equiv \frac{Dd}{D\,t_p} = B_1 + B_2\,p^n \qquad \text{and} \qquad \left(\dot{m}\right)_d = (1 - \boldsymbol{a})\frac{S_p}{V_p}\dot{d} \qquad (17),(18)$$

It should be noted that only one of Equation 16 and 17 has to be solved at each point according to the temperature being less than or equal to the ignition temperature, respectively.

Numerical Model

The balance equations, described above, constitute a system of coupled partial differential equations that can be solved using a finite-difference technique. The derivatives in these equations are converted to algebraic expressions that pertain to a rectangular mesh of discrete, ordered points distributed about the geometry. Non-orthogonal geometric surfaces are handled using virtual cells, part of which may be occluded within geometric surfaces. Values of the dependent variables are determined at the cell centers using an iterative numerical method in space and time. An explicit method is chosen since the resolution of boundary layers (either on the chamber walls or the particle surfaces) is not considered. The numerical time step is limited by characteristic cell dimension and the fastest wavespeed (i.e., the Courant condition) except near the mesh boundaries where a virtual cell technique is applied. The Courant condition is not overly restrictive for the present class of gas dynamic problems since the need for wave tracking is apparent and thereby integration using Courant numbers larger than unity is not desirable.

The spatial values of the dependent variables at each time step are determined by a numerical integration method, denoted the Continuum Flow Solver (CFS), which treats the continuous phase and certain of the discrete phases in an Eulerian fashion. The Flux-Corrected Transport (FCT) scheme [9]

is a suitable basis for the CFS since the method is explicit and has been shown to adapt easily to massively parallel systems [10]. The discrete phases are treated by a Lagrangian formulation, denoted the Large Particle Integrator (LPI), which tracks the particles explicitly and smoothes discontinuities associated with boundaries between propellants yielding a continuous distribution of porosity over the entire domain. The manner of coupling between the CFS and the LPI is through the attribution of properties (e.g., porosity, mass generation) at points in the flow. The size of the grid as well as the number of Lagrangian particles is user prescribed.

Continuum Phase

The Flux-Corrected Transport Algorithm LCPFCT [9] forms the basis for the CFS. The Virtual Cell Principle [11] can be used as a means of accommodating arbitrary boundary geometries within a uniform, structured, rectangular mesh. In the present work use is made of mesh boundary cells that are partially occluded by the domain boundaries and as such are reduced in size, thus requiring the application of a local characteristic analysis to insure numerical stability [12]. LCPFCT is a one-dimensional solver for a canonical balance equation in the form,

$$\frac{\partial \boldsymbol{r}}{\partial t} = -\frac{1}{r^{k-1}}\frac{\partial}{\partial r}\left(r^{k-1}\boldsymbol{r}v\right) - \frac{1}{r^{k-1}}\left(r^{k-1}D_1\right) + C_2\frac{\partial D_2}{\partial r} + D_3 \tag{19}$$

where k = 1, 2 or 3 for planar, cylindrical and spherical flows respectively. Here ρ is the transported variable and D_1, D_2, and D_3 and are referred to as source terms. The computational domain is decomposed into N cells. The state variable ρ_i is considered to apply to the center of the i-th cell. The cell has volume Λ_i and is bounded by surfaces whose areas are $A_{i-1/2}$ and $A_{i+1/2}$ which are presumed to be orthogonal to the fluid streamline. Fluid properties on the cell boundaries are determined by averaging with the values in adjacent cells. Equation 19 is integrated according to a finite volume formulation via several steps in which strong diffusion is first introduced and then subsequently canceled by antidiffusion to the maximum extent consistent with the minimal requirements of computational stability and the condition that the antidiffusion not introduce new maxima or minima in the updated distribution of ρ.   As discussed by Boris et al. [9] LCPFCT may be made second order accurate in time by using a two-step scheme, first integrating from t to t + Δt/2 and then from t to t+Δt using the intermediate values to define the geometric terms and the source terms. Further, LCPFCT is applied to multidimensional situations by timesplitting, integrating first in one direction and then another with the appropriate subsets of the multi-dimensional equations. Referring to the system of equations for the continuous phase, Equations 1-6, it is easy to see that each of these is of the form of Equation 19 with the proper choices of ρ, D_1, D_2, D_3 and k. However, while a natural set of choices for the fluxes would be $\alpha\rho$, $\alpha\rho Y_j$, $\alpha\rho u$, $\alpha\rho v$, and αe, we have elected to use ρ, ρY_j, ρu, ρv, and e folding the influence of the porosity, α, into the metric quantities $A_{i+1/2}$ and $A_{i+1/2}$. This selection yields smooth thermodynamic state variables and minimizes the influence of the diffusive step in the algorithm.

Discrete Phase

Numerical representation of the discrete phase is assigned to the Large Particle Integrator (LPI). The LPI is intended to be applied to those discrete phases that cannot be assumed to be in

mechanical equilibrium with the continuous phase. In all cases of practical interest this will include all solid propellant increments. Recall that we adopt the nomenclature of charge "increment" to mean distinct subcharges (or modules) that are usually subcaliber (i.e., of radial dimension smaller than that of the chamber). The increment walls comprise the propellant boundaries (with ullage between these walls and the chamber walls). In the case where the propellant fills the gun chamber, then there are no increments and the propellant boundaries are coincident with the chamber walls. In either case the propellant boundaries are tracked explicitly via the adoption of a Lagrangian representation. These boundaries are not viewed as discontinuities thus the porosity is made to vary continuously over a short distance and internal jump conditions are not applied. Continuum flow resistance due to these boundaries is attributed to boundary LPI particles. A condition of non-penetration by the continuous phase is imposed on the CFS until a state of overpressure is reached and the boundaries are assumed to yield. The CFS is required to be robust enough to integrate the flow in a stable manner in the presence of strong porosity gradients resulting from this treatment; LCPFCT meets this requirement.

Consider a single charge increment defined by a rear and forward delimiter and by an inner and an outer delimiter. The increment is assumed to occupy uniformly the cylindrical domain defined by these delimiters minus any intrusions by the chamber walls. The increment is then represented by a structured array of LPI-particles. These are arranged in an axially uniform manner from the rear to the forward delimiter and radially from the inner to the outer delimiter. Each particle is assigned a weight as follows. The grain number density, n_b, may be computed from $n_b = M_i / (\rho_p V_p V_i)$, where M_i is the increment mass and V_i the increment volume and ρ_p, V_p, are respectively the density of the propellant and the initial volume of an individual grain. Then the number weighting of a particle is taken to be n_b times the volume of a cylinder defined by the midpoints between the particle and its four neighbors. For boundary particles the relevant midpoint value is replaced by the appropriate axial or radial coordinate of the particle. It is easy to see that this process automatically assigns non-zero weight to at most one particle that was pushed into contact with a radial boundary. In addition to number weighting, each LPI-particle is assigned the following attributes: axial/radial position, velocity, surface regression and temperature, cubic profile thermal parameter (Eq. 15), porosity, and intergranular stress.

At each time step, Equation 6 is integrated using a simple first order time differencing scheme. The pressure gradient is computed on the continuum mesh by means of central differencing to define cell centered values. Then for each LPI-particle a local value of pressure gradient, together with all other necessary continuous phase state variables, is computed using linear interpolation in both the radial and the axial directions. The positions are updated first for all LPI-particles. Then, in a second sweep the velocities are updated and subjected to the external boundary condition. Depending on the surface temperature either the thermal parameter (Equation 16) or the surface regression (Equation 17) is integrated. In the same sweep all the interphase transfer properties (see Constitutive Laws for the Discrete Phase) are computed for each particle. The gradient of intergranular stress is computed using differences between the LPI-particles that neighbor the particle in question. One-sided differences are used at boundaries. Field properties determined by the LPI are mapped onto the grid for the continuum flow solver together with the porosity distributions as follows. At each time step each particle is

assigned a rectangular domain of influence. Let z_L and z_R be the left and right axial delimiters and r_i and r_o be the inner and outer delimiters. Let the coordinates of the particle be $(z_{ij}, r_{i,j})$ and let,

$$V_{ij} = \frac{\boldsymbol{p}}{8}(z_R - z_L)\left[(r_{ij} + r_o)^2 - (r_{ij} + r_i)^2\right] \tag{20}$$

be the volume associated with the particle. If $V_{p,ij}$ and N_{ij} are respectively the grain volume and the number weighting, we can define the particle volume fraction, $\alpha_{ij} = V_{p,\,ij}\,N_{ij}\,/\,V_{ij}$ and similarly for the other interphase data such as mass and enthalpy transfer and drag. The value of α_{ij} so defined is used to update the solid propellant intergranular stress by means of a simple first order time difference. To assign the LPI-particle volume to the continuum mesh we simply scan the continuum mesh to find those cells whose centers are in the domain of influence. Let (z_c, r_c) be the coordinates of such a cell center. Define,

$$w_z = \left\{ \frac{z_R - z_C}{z_R - z_{ij}} \text{ for } (z_C \geq z_{ij}) \quad ; \quad \frac{z_C - z_L}{z_{ij} - z_L} \text{ for } (z_C < z_{ij}) \right\}$$

and define w_R analogously for the radial direction. Then the continuum cell in question is assigned a volume fraction contribution $w_R w_Z \alpha_{ij}$ and similarly for the other interphase properties. These values are summed over all LPI-particles. It is not hard to see that this is tantamount to a bidirectional linear interpolation process. It is also clear that the procedure described in this section results in an implicit integration of the mass balance given by Equation 5.

Accomplishments

Numerical simulations of the MACS as well as ETC-ignited HLD charges being designed for the FCS have been performed using HPCs. Significant progress has been made toward accomplishing the Grand Challenge as outlined at the beginning of this paper. In this introduction, a list of those accomplishments is provided. Unfortunately, graphical results of the simulations leading to these accomplishments cannot be provided in this public-release paper. As both a substitute and as a means of demonstrating the NGEN3 code, this section does include several illustrative examples of both MACS-type and HLD charges.

The NGEN3 code was utilized for the XM297 Crusader Cannon and the MACS propelling charge increments that are under development by PM-Crusader and PM-Crusader/Munitions. Three accomplishments are: **(1)** NGEN3 simulations for the XM231, low-zone MACS charge, displayed the importance of non-sequential centercore charge ignition, module movement and case ignition/burn-through, 2D and 3D propellant flamespreading behavior within the modules, module cap separation, and non-sequential module bursting [13]. These simulations are aiding in the type classification of the charge. **(2)** The NGEN3 code was used to uncover a heretofore-unknown physical phenomenon for the XM232 high-zone MACS charge that only occurs during charge fallback in an elevated gun tube. NGEN3 simulations of these charges proved that a prevailing gas dynamic process, when the modular charges are positioned adjacent to the gun chamber breech face would cause the rigid charges modules to be displaced forward. This displacement mitigates any pressure wave formation that would have occurred had the charges remained on the breech face during flamespreading and rupture [13].

Laboratory fixture tests, conducted at ARL, validated the code. Subsequently, the NGEN simulations for the XM232 were used to plan range testing of the XM297 cannon at YPG. The YPG gun tests confirmed that XM232 increments at Zones 4 – 6 positioned adjacent to the wedge face support predictions by the NGEN code; the ballistic cycle is virtually unchanged, except for slight differences in timing. (**3**) NGEN3 code simulations for the XM232 charge uncovered a heretofore-unknown physical phenomenon involving the importance of case combustion. In was found that case combustion is clearly a significant contributor to chamber pressure and a significant factor in the generation of pressure differentials in the gun chamber. NGEN3 simulations indicate that the prediction of pressure differentials that are similar to those measured in the gun firings are not possible without first achieving good agreement with measured pressure data early in the ballistic cycle and including the effects of case combustion [14].

In other applications of the NGEN3 code, for direct-fire gun systems, solid propellant charges ignited using conventional and ETC igniters were simulated using the NGEN code. Simulations of 60mm [15] and 120mm tank charges composed of disk and granular solid propellant media demonstrated the ability of the NGEN code to accommodate ignition and flamespreading through a novel charge including the effects of projectile afterbody intrusion and movement as well as compression and the resulting ignition delay in the propellant. These simulations revealed that the igniter, positioned at the gun breech, could be so forceful as to compress the disk charge, closing critical flow paths in the charge and preventing effective flamespreading and even ignition. These simulations showed that the low molecular weight plasma, generated by an ETC igniter, could circumvent this problem by establishing a convectively driven flame that propagates faster than the material compression wave in the disk propellant thereby permitting an even ignition of the charge. A basic design tenet for using HLD charges was established, namely pressure waves in the chamber generated by the conventional igniter, when paired with the disk propellant charge, were avoided by using an ETC igniter.

Results for a Typical Indirect-Fire Gun Chamber

Figure 1A shows a schematic of the gun chamber filled with granular propellant. Since the configuration is axisymmetric, only one radial plane is displayed that extends from the chamber centerline (y=0) to the outer wall (sloped from 8.4cm to 8.1cm). The axial extent, from the breech to the projectile base, is 106cm (the gun tube extends beyond this point for an additional 594cm). The projectile mass is 44kg and resists movement for the first 5cm of travel. The granular propellant is cylindrical (physical characteristics are available from the author). The porosity of the propellant bed is 0.63.

Figures 1B and 1C show alternate arrangements in which the granular propellant is packaged in either one or two cylindrical modules. These modules are assumed to be aligned along the centerline of the chamber and to consist of a main charge section (porosity of 0.63) and a centercore that is filled with ball propellant with properties that are distinct from the granular propellant (porosity of 0.4). The module are sealed with walls that are rigid but permeable, admitting flow (or "leaking") only after a significant gas pressure differential has been reached. Subsequently, these walls are allowed to break or

"burst" after a fixed time interval has elapsed since over pressurizing. A rigid body analysis is enforced up to the instant of container bursting. These walls can resist substantial pressure loading except for the radial wall separating the main charge from the centercore (i.e., an internal wall) and the axial wall that represents a module cap that is used to fill the modules. This cap is located at the module end closest to the chamber breech. However, breakage of the internal wall or the module cap does not relax the rigid body treatment of the remaining module components. In each case the charge is ignited at the breech end, near the chamber centerline over 2cm of length, 3cm in radius and during the first 6ms.
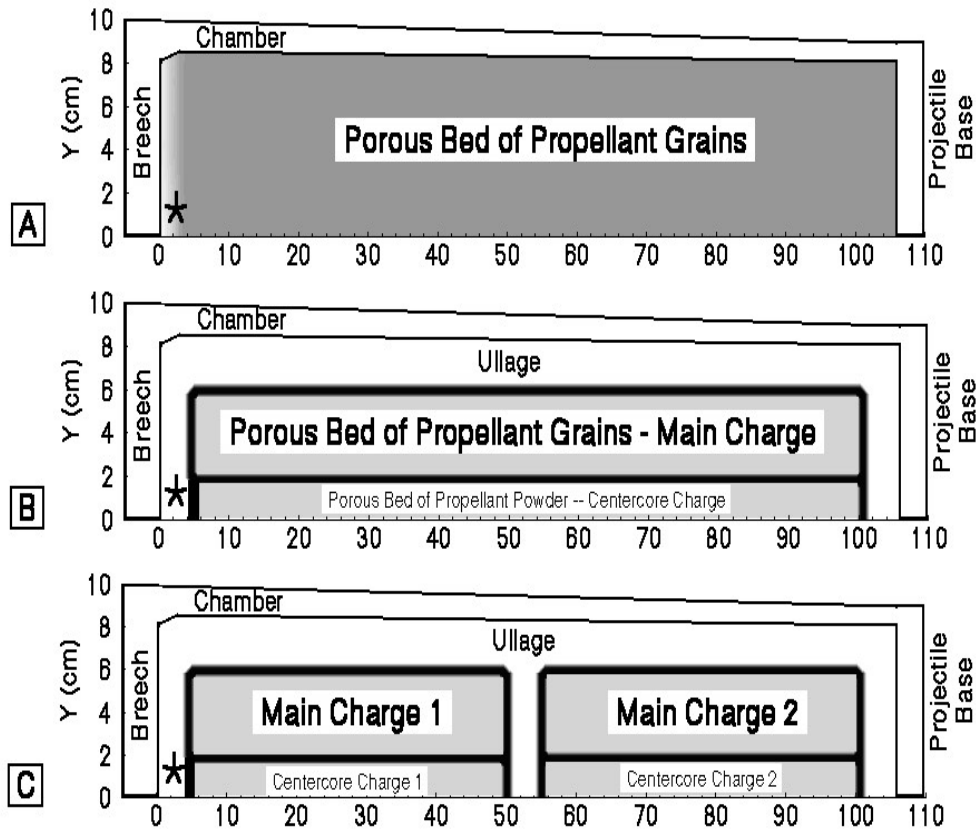
Figure 1. Schematics of Gun Charge Configurations: A) Loose Charge, B) Packaged Charge in Single Module, C) Packaged Charge in Two Modules. Ignition Source Indicated by (*).

Figure 2 summarizes the computed results for the one module charge (Fig. 1B). The breech-end igniter starts a flame that quickly opens the centercore and ignites the ball propellant; gas flows into the radial ullage region (Fig. 2A,B). After about 3ms, the centercore is fully ignited, flow is filling the ullage near the projectile, and the internal wall separating the centercore from the main charge is opening (Fig. 2C,D). By 6ms the main charge is fully open and partially ignited (Fig. 2E,F). Increased pressurization of the module causes the module cap to separate (Fig. 2G) and gas flow to exit the module at high velocity against the breech face.

Figure 3 summarizes the computed results for the packaged charge of two modules (Fig. 1C). The breech-end igniter starts an ignition wave or flame that quickly opens and ignites the first centercore

(Fig. 3A-D). Gas flow fills the ullage regions in the chamber and bursts into the second centercore but fails to ignite the ball propellant at this time (Fig. 3D). By 8ms the main charge of module 1 is open and partially burning (Fig. 3E,F) emitting hot flow that ignites the second centercore. A pressure wave, traveling though the radial ullage and into the region near the projectile base, over pressurizes and bursts the second centercore at its far axial end (Fig. 3E). As a result, main charge flamespreading in the second module begins nearest to the projectile base (Fig. 3H). By 11ms the main charge of the first module is fully ignited causing increased pressure that bursts the endcap, causing high velocity flow against the breech face (Fig. 3G) and a sudden
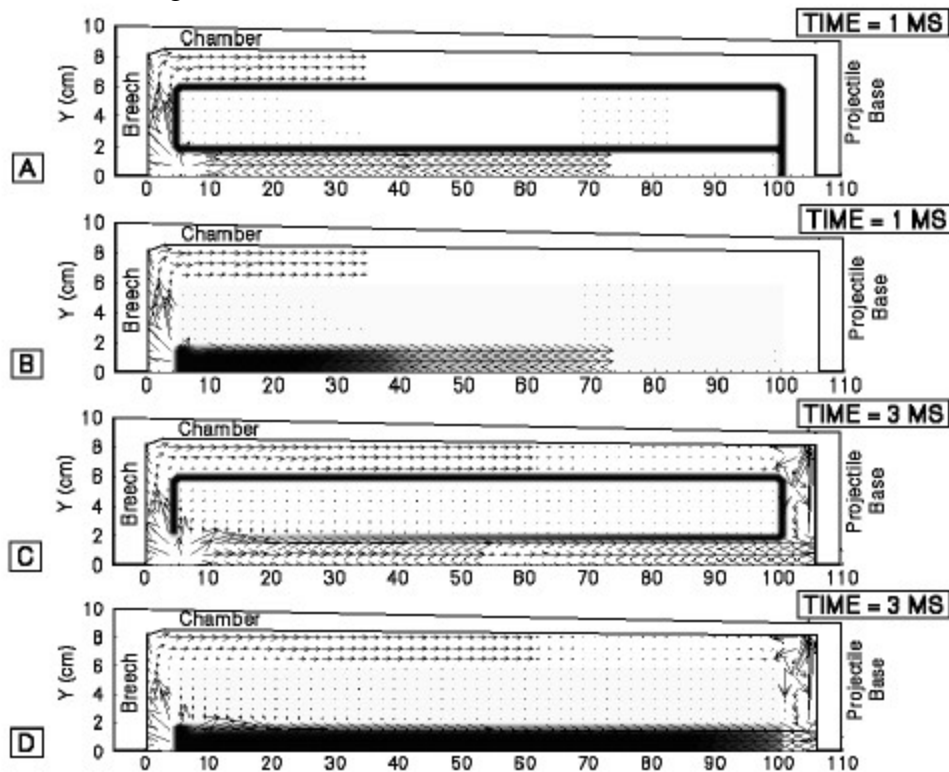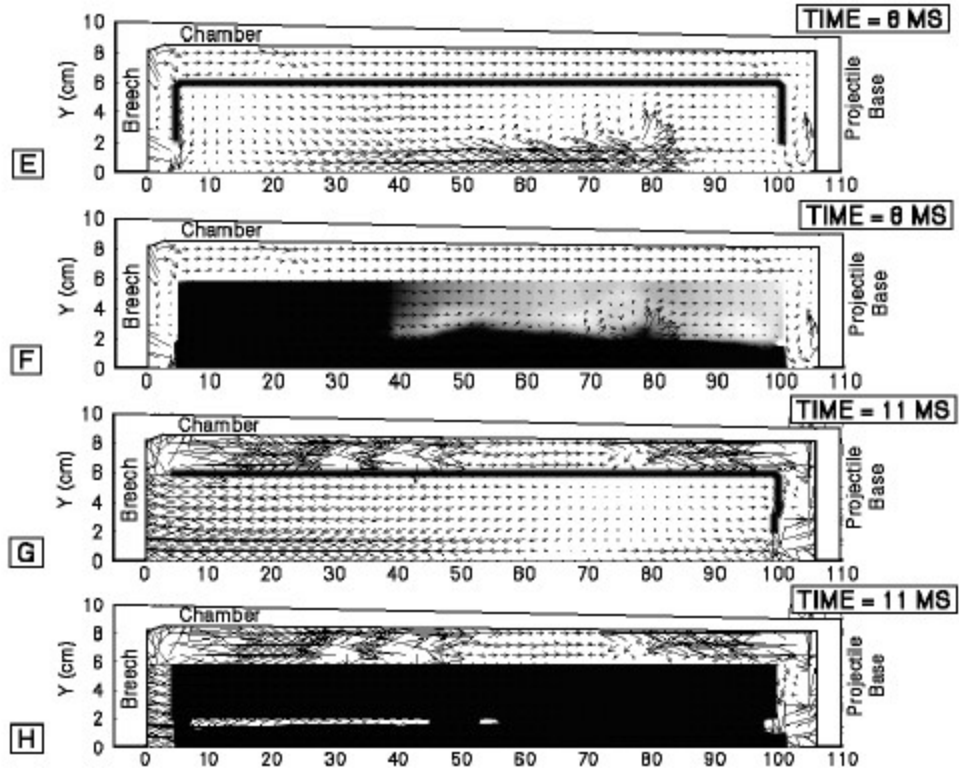
Figure 2. Computed Results for Packaged Charge (1 module): A,B) Time = 1ms; C,D) Time = 3ms; E,F) Time = 8ms; G,H) Time = 11ms. Gas Velocity Vectors along with Module Boundaries (A,C,E,G) and Propellant Temperature Contours (B,D,F,H) ranging from 294K (white) to 440K (black).
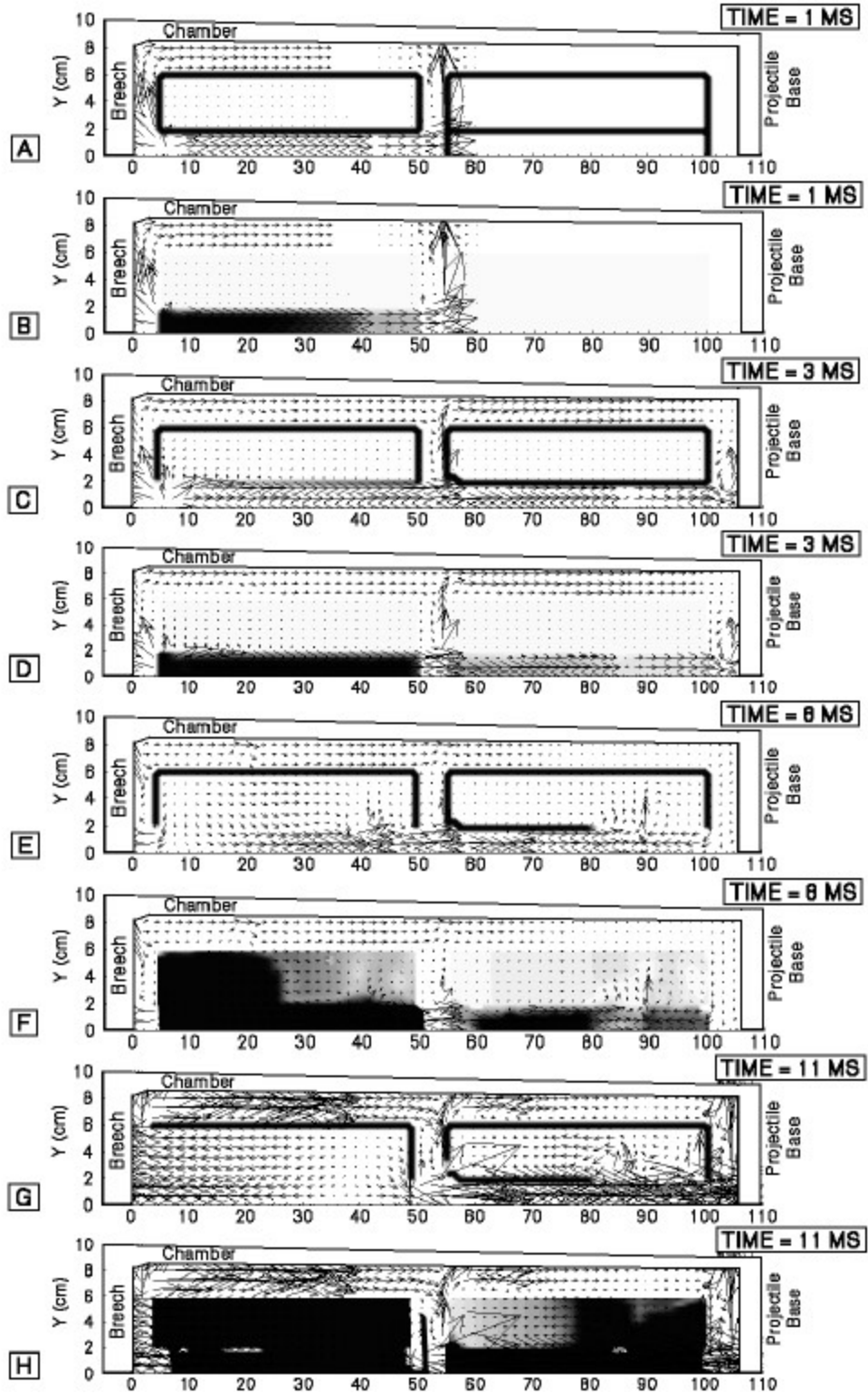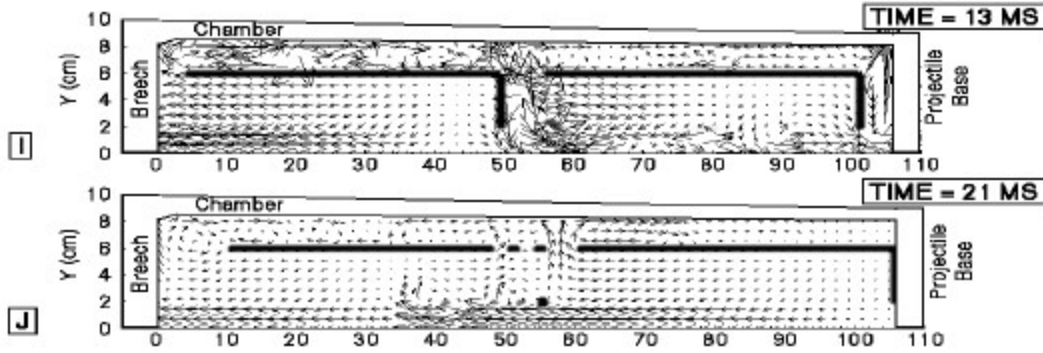
Figure 3. Computed Results for Packaged Charge (2 modules): A,B) Time = 1ms; C,D) Time = 3ms; E,F) Time = 8ms; G,H) Time = 11 ms. Gas Velocity Vectors along with Module Boundaries (A,C,E,G) and Propellant Temperature Contours (B,D,F,H) from 294K (white) to 440K (black).

Figure 3 -- continued. Computed Results for Packaged Charge (2 modules): I) Time = 13ms; J) Time = 21ms. Gas Velocity Vectors along with Module Boundaries.

forward movement of the first module. This movement increases the pressure against the endcap of the second module and causes it to burst (Fig. 3I). These events cause the second module to move forward and impact the projectile base (Fig. 3J).

The pressure histories of the events described in Figures 2 and 3 are shown in Figures 4 and 5. For the case of two modules (Figure 5) the breech pressure is slowly increasing nearly coincident with projectile base pressure (zero pressure differential) until about 10ms. Subsequently, the base pressure increases rapidly (-1.5MPa pressure differential) in response to pressure waves caused by the initial disintegration of the first module and the igniting of the second. Between 11ms and 18ms a series of three pressure waves (seen as repeating positive, +1 MPa, and negative, -1 MPa, pressure differentials) is caused by the movement and breakup of the modules. Another negative pressure differential (-2.5MPa) occurs at 21ms due to the impact of the second module upon the projectile base. After this time the now loose propellant is free to move within the chamber and these waves subside (note positive differential after 22ms in Fig. 5).
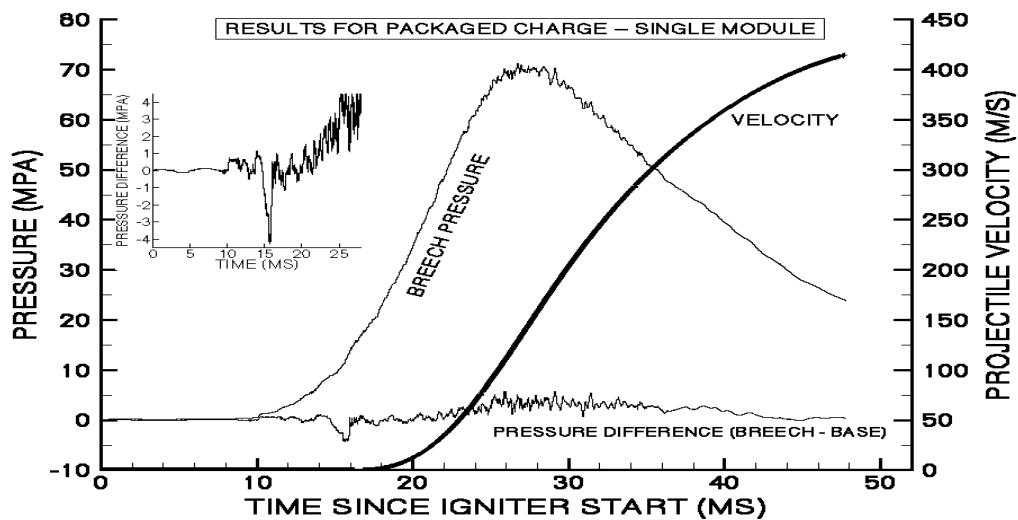

Figure 4. Computed Results for Packaged Charge (1 module): Projectile Velocity, Breech Pressure and Pressure Difference (Breech Pressure Minus Projectile Base Pressure) vs. Time.
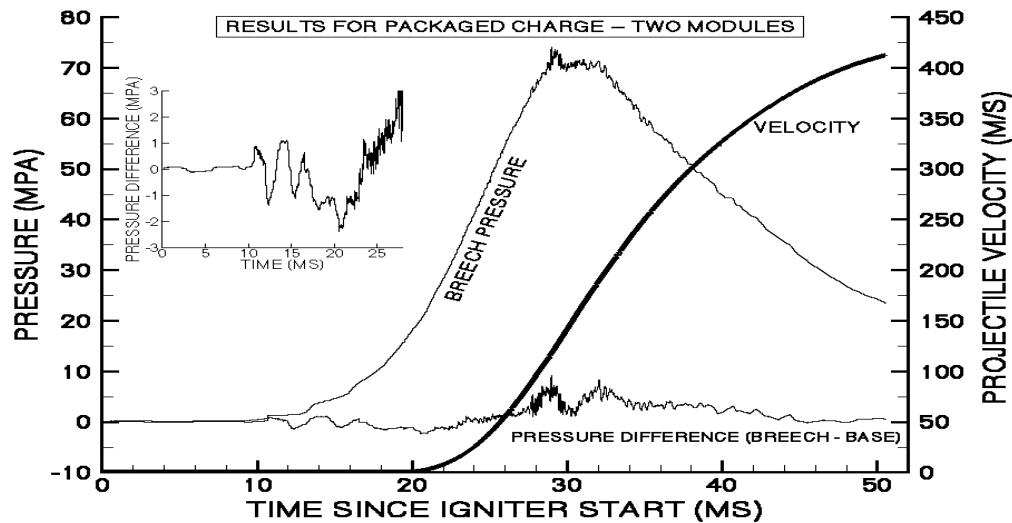
Figure 5. Computed Results for Packaged Charge (2 modules): Projectile Velocity, Breech Pressure and Pressure Difference (Breech Pressure Minus Projectile Base Pressure) vs. Time.

Results for a Typical Direct-Fire Gun Chamber

Figure 6 shows the computed porosity contours (white to black: open space to nearly solid material) and propellant temperature contours (white to black: ambient to 440K) for a 120mm HLD charge consisting of separate regions of disk and granular propellant. The propellant disks are stacked axially in the chamber; each disk has an inner radius that provides space for the igniter and the projectile afterbody and outer radius that is smaller than the radius of the chamber (shown from centerline to chamber wall). Figure 6A shows the initial condition of the charge (i.e., before the igniter is activated). Figures 6B and 6C show the condition after 6ms (note that the projectile has moved into the gun tube and out of view). It can be noted that the granular propellant has been consumed and that the stack of disks has been pushed forward but is not fully ignited (Figure 6C). There is a region of disks that have been compressed forward (from 50-55cm in Fig. 6B) and thus the interstitial gaps have been closed preventing convective heat transfer. When this simulation is repeated using an ETC igniter, plasma convection is accomplished between all disks before significant disk compression and thus the entire stack of disk propellant is efficiently ignited.

Figures 7 shows the computed porosity and pressure contours for a 60mm chamber with two regions of SP disks. The propellant disks are stacked axially in the chamber; each disk has an inner radius that provides space for a centercore ullage region (that permits the flow of igniter/plasma gases) and outer radius that is smaller then the radius of the chamber (shown from centerline to chamber wall). Figures 7A and 7B show the early time (0.5ms) condition of the charge. Figures 7C and 7D show the condition after 5ms. It can be noted that pressurization of the rearmost region of disks occurs in the center of that region (Figure 7B) – pressure first increases in the center and one can observe flow

18

streaming from the center into the ullage region below the disks. This region has not ignited (the porosity contours of Figure 7A show no drop in
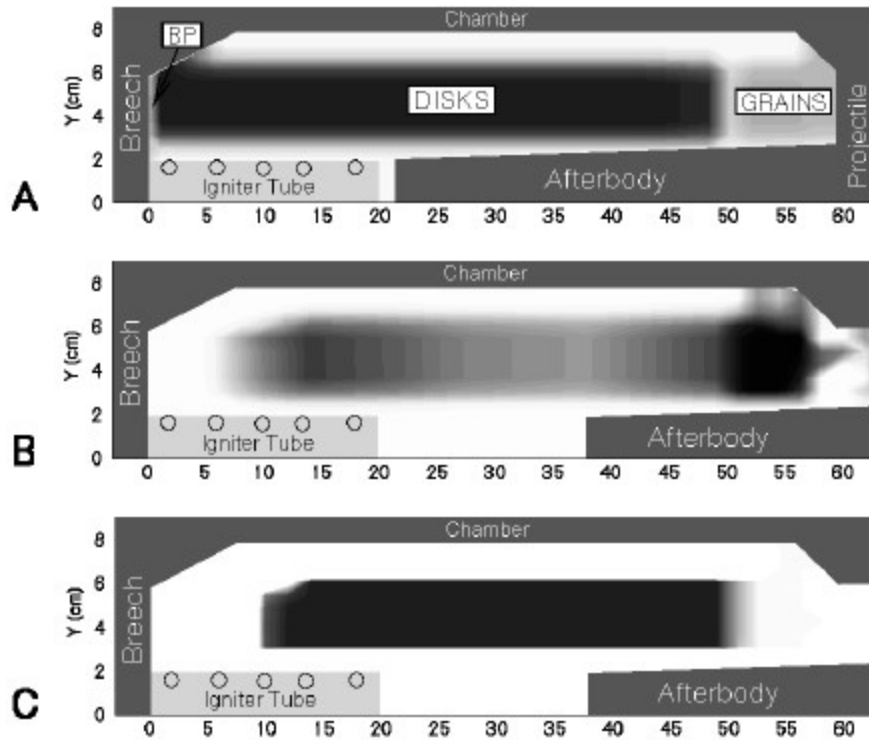

Figure 6. Computed Results for 120mm High-Loading Density Charge (SP disks & grains): A) Porosity Contours (black is dense material) at Initial Time; B) Porosity Contours at 6ms; C) Propellant Temperature Contours (black is ignited propellant at 440K) at 6ms.

porosity at the center of the region at this time). It is here that the flow confinement is the smallest (i.e., away from the breech face), at least initially, and the igniter gases can flow somewhat freely. Later in time, a significant pressurization occurs at the rear of the rearmost region of disks (Figure 7D) caused by propellant ignition (i.e., the porosity contours of Figure 7C show that the disks are being consumed). This is the breech ignition process and is not usually desirable in HLD charges since this condition can cause the disks to compress up against the projectile base, retarding flamespreading through the charge. In this case, the loading density is high enough that with little ullage in the chamber for pressure relief, the breech face of the chamber is being inappropriately stressed. It is clear that for HLD charges of this type, some charge reconfiguration is required in order to achieve efficient charge ignition and combustion.

Summary

The Army Research Laboratory has developed a scaleable, 3D, multiphase, computational fluid dynamics (CFD) code with application to gun propulsion (interior ballistics) modeling. The NGEN3 code, which incorporates general continuum equations along with auxiliary relations into a modular code structure, is transportable between computer architectures and is applicable to a wide variety of gun

propulsion systems. Two such systems are the Army's Modular Artillery Charge System (MACS) and the Future Combat System (FCS). NGEN3 code development and application to the MACS and FCS is currently a DoD HPC Grand Challenge (No. 112) and
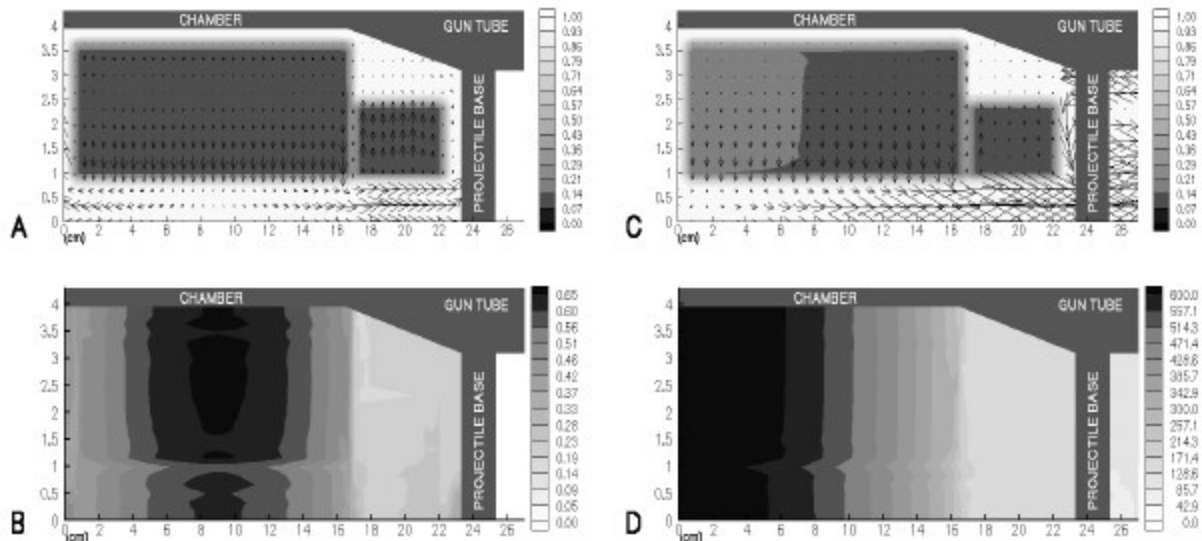

Figure 7. Computed Results for 60mm High-Loading Density Charge (two regions of SP disks): A) Porosity Contours and Velocity Vectors at 0.5ms; B) Pressure Contours at 0.5ms; C) Porosity Contours and Velocity Vectors at 5ms; D) Pressure Contours at 5ms.

significant progress has been made to date. The progress report given in this paper demonstrates the utility of DoD high performance computers (HPCs) in meeting this challenge.

Acknowledgements

References

[1] Nusca, M.J., and Gough, P.S., "Numerical Model of Multiphase Flows Applied to Solid Propellant Combustion in Gun Systems," Proc. of the 34th AIAA Joint Propulsion Conference, AIAA Paper 98-3695, July 1998.

[2] Nusca, M.J., "Computational Fluid Dynamics Model of Multiphase Flows Applied to Solid Propellant Combustion in Gun Systems," Proceedings of the 18th International Symposium on Ballistics, San Antonio, TX, 1999, pp. 252-261.

[3] Nusca, M.J., "Numerical Model of Multiphase Flows Applied to Solid Propellant Combustion in Gun Systems," Journal of Propulsion and Power, to appear 2001.

[4] Gough, P.S., and Zwarts, F.J., "Modeling Heterogeneous Two-Phase Reacting Flow," AIAA Journal, Vol. 17, No. 1, January 1979, pp. 17-25.

[5] Gough, P.S., "Modeling Two-Phase Flow in Guns," Interior Ballistics of Guns, Edited by H. Krier, American Institute of Aeronautics and Astronautics, New York, 1979.

[6] Williams, F.A., Combustion Theory, Addison-Wesley, 1965.

 [7] Kooker, D.E., Sandusky, H.W., Elban, W.L., and Conroy, P.J., "Full-Scale Quasi-Static Compaction of Granular Solid Propellant," ," Proc. of the 31st JANNAF Combustion Mtg, CPIA Pub. No. 620, Vol. 1, Oct. 1994, pp. 201-225.

[8] Gelperin, N.I. and Einstein, V.G., "Heat Transfer in Fluidized Beds," Fluidization, edited by Davidson, J.F. and Harrison, D., Academic Press, NY, 1971.

[9] Boris, J.P., Landsberg, A.M., Oran, E.S., and Gardner, J.H., "LCPFCT -- A Flux-Corrected Transport Algorithm for Solving Generalized Continuity Equations," Naval Research Laboratory MR/6410-93-7192, April 16, 1993.

[10] Oran, E.S., Boris, J.P. and Brown, E.F. "Fluid-Dynamic Computations on a Connection Machine -- Preliminary Timings and Complex Boundary Conditions," AIAA Paper 90-0335.

[11] Landsberg, A.M., and Boris, J.P., "The Virtual Cell Embedding Method: A Simple Approach for Gridding Complex Geometries,"AIAA Paper 97-1982.

[12] Gough, P.S., "Development of Next-Generation Interior Ballistics Code II. Applicability to Various Propulsion Systems," Proc. of the 31st JANNAF Combustion Meeting, CPIA Pub. No. 620, Vol. 1, Oct. 1994, pp. 257-278.

[13] Nusca, M.J., "Investigation of Ignition and Flamespreading Dynamics in the Modular Charge Artillery System Using the NGEN Multiphase CFD Code," Proc. of the 36th JANNAF Combustion Subcommittee Meeting, Oct. 1999.

[14] Nusca, M.J., "Numerical Modeling of the Modular Artillery Charge System Using the NGEN Multiphase CFD Code – Effects of Case Combustion," Proc. of the 37th JANNAF Combustion Subcommittee Meeting, November 2000.

[15] Conroy, P.J., and Nusca, M.J., "Interior Ballistics Modeling of High-Loading Density Charges in an ETC Gun Using the NGEN Multiphase CFD Code, " Proc. of the 37th JANNAF Combustion Subcommittee Meeting, Nov. 2000.